Wall-mode instability in plane shear flow of viscoelastic fluid over a deformable solid

Paresh Chokshi,[1,*] Piyush Bhade,[1] and V. Kumaran[2]
[1]*Department of Chemical Engineering, Indian Institute of Technology Delhi, New Delhi 110016, India*
[2]*Department of Chemical Engineering, Indian Institute of Science, Bangalore 560012, India*
(Received 27 October 2014; published 10 February 2015)

The linear stability analysis of a plane Couette flow of an Oldroyd-B viscoelastic fluid past a flexible solid medium is carried out to investigate the role of polymer addition in the stability behavior. The system consists of a viscoelastic fluid layer of thickness R, density ρ, viscosity η, relaxation time λ, and retardation time $\beta\lambda$ flowing past a linear elastic solid medium of thickness HR, density ρ, and shear modulus G. The emphasis is on the high-Reynolds-number *wall-mode* instability, which has recently been shown in experiments to destabilize the laminar flow of Newtonian fluids in soft-walled tubes and channels at a significantly lower Reynolds number than that for flows in rigid conduits. For Newtonian fluids, the linear stability studies have shown that the wall modes become unstable when flow Reynolds number exceeds a certain critical value Re_c which scales as $\Sigma^{3/4}$, where Reynolds number $\mathrm{Re} = \rho V R/\eta$, V is the top-plate velocity, and dimensionless parameter $\Sigma = \rho G R^2/\eta^2$ characterizes the fluid-solid system. For high-Reynolds-number flow, the addition of polymer tends to decrease the critical Reynolds number in comparison to that for the Newtonian fluid, indicating a destabilizing role for fluid viscoelasticity. Numerical calculations show that the critical Reynolds number could be decreased by up to a factor of 10 by the addition of small amount of polymer. The critical Reynolds number follows the same scaling $\mathrm{Re}_c \sim \Sigma^{3/4}$ as the wall modes for a Newtonian fluid for very high Reynolds number. However, for moderate Reynolds number, there exists a narrow region in β-H parametric space, corresponding to very dilute polymer solution ($0.9 \lesssim \beta < 1$) and thin solids ($H \lesssim 1.1$), in which the addition of polymer tends to increase the critical Reynolds number in comparison to the Newtonian fluid. Thus, Reynolds number and polymer properties can be tailored to either increase or decrease the critical Reynolds number for unstable modes, thus providing an additional degree of control over the laminar-turbulent transition.

DOI: 10.1103/PhysRevE.91.023007 PACS number(s): 47.35.−i, 47.20.Ft, 83.60.Df, 83.60.Bc

I. INTRODUCTION

The flow past compliant surface is of great practical importance in medicine and bioengineering applications as well as in microfluidic systems fabricated using soft materials. Blood, the fluid in cardiovascular flows, is shear thinning and viscoelastic. The viscoelasticity introduces an additional time scale, the fluid relaxation time, which significantly alters the flow dynamics. In microfluidic applications as well, we encounter systems where the fluids are viscoelastic due to polymeric additives. For a flow through rigid pipes, an addition of small amount of polymer to otherwise Newtonian fluid is known to suppress the turbulence, leading to significant drag reduction at high Reynolds number. Similarly, it might be expected that addition of small amounts of polymers, to render the fluid viscoelastic, could play a significant role in the laminar-turbulent transition. The Newtonian flow past through deformable channels or tubes at high Reynolds number is known to undergo transition when the wall shear modulus is lower than a certain critical value [1–3]. It would be interesting to examine how this instability will be affected by addition of small amount of polymer. The complete suppression of the instability or delay in flow transition like in a rigid tube could be highly beneficial in designing the flow channels with a flexible wall.

The dynamics of fluid flow past a deformable surface qualitatively differs from that of rigid surface because of the coupling between the fluid and wall dynamics, and the elasticity of the surface could affect the fluid flow. This elastohydrodynamic coupling could influence the transition from laminar to turbulent flow in such systems. The experiments conducted by Krindel and Silberberg [4] indicated that the onset of laminar-to-turbulence transition in Newtonian flow through gel-walled tube can occur at Reynolds number much smaller than 2100, the critical Reynolds number for the flow through rigid tube. Motivated by this observation, extensive studies pertaining to the linear stability analysis of fluid flow in tubes and channels bounded by flexible walls have been carried out. The results of theses studies indicated that there are at least three modes of instability in flexible-walled tubes and channels which qualitatively differ from those in rigid tubes and channels, namely *viscous modes*, *wall modes*, and *inviscid modes*, depending upon the regime of flow operation. An excellent review and classification of these instabilities has been covered by Kumaran [5].

The relevant studies for the Newtonian fluid will be reviewed first. With the help of linear stability analysis, Kumaran *et al.* [6] predicted that the coupling between fluid flow and wall dynamics renders the flow unstable even in the absence of inertia. For plane Couette flow with shear rate V/R, the viscous instability sets in when the dimensionless shear rate $V\eta/GR$ exceeds a critical value. Here η is the viscosity of the fluid, R is the channel width, and G is the shear modulus of the gel wall. Similar analysis of viscous instability mode in flow past flexible surface has been carried out for Hagen-Poiseuille flow through tube [7] and plane Poiseuille flow through channel [8]. Experiments conducted using a layer of silicon

*paresh@chemical.iitd.ac.in

oil supported on cross-linked polydimethylsiloxane gel in a parallel-plate rheometer have quantitatively confirmed the presence of instability [9–11]. The destabilizing mechanism is proposed to be the transfer of energy from the mean flow to the fluctuations due to the shear work done by the mean flow at the interface.

At very high Reynolds number, there exists a class of solution to the stability problem, known as "wall modes," where the vorticity in the fluid is confined to a thin layer near the fluid-solid interface. Simple scaling arguments show that the thickness of this wall layer is $O(k\mathrm{Re})^{-1/3}$ smaller than that for large values of $k\mathrm{Re}$, where k is the axial wave number scaled with the channel width and the Reynolds number, Re, is defined based on maximum fluid velocity. For $k \sim 1$, which is the regime of investigation in the present study, the time rate of damping or growth of these modes is $O(\mathrm{Re}^{-1/3})$ smaller than the strain rate in the fluid. These modes were first studied by Corcos and Sellars [12], Gill [13], and Gill [14] for Hagen-Poiseuille flow of in rigid tube and their asymptotic studies of linear stability showed that wall modes are always stable in rigid tube. Since the disturbance is confined to a layer close to the wall that is much smaller than the pipe diameter, the wall of the pipe can be well approximated as a flat surface and the linear velocity profile can be assumed for the mean flow in the wall layer. Therefore, wall modes in plane Couette flow are same as that in pipe flow and hence are stable to infinitesimal disturbances. Based on the expectation that the influence of wall elasticity should be strong on the wall layer, Shankar and Kumaran [15] and Shankar and Kumaran [3] carried out the asymptotic analysis using $O(\mathrm{Re}^{-1/3})$ as small parameter in the regime $\mathrm{Re} \gg 1$ and showed that wall modes are unstable for flow past a flexible surface. This analysis captures all the modes obtained by numerical solution [2,16,17] and estimates the critical Reynolds number, Re_c, for a given fluid-gel wall system specified by a velocity-independent dimensionless parameter $\Sigma = \rho G R^2/\eta^2$. The neutral stability curve in the Re-Σ plane follows the power-law relation $\mathrm{Re} \sim \Sigma^{\alpha}$. In the limit of $\Sigma \gg 1$, it has been shown that exponent $\alpha \approx 3/4$. Recent experiments by Verma and Kumaran [18] and Verma and Kumaran [19] demonstrate that the flow through flexible tube undergoes transition from a parabolic laminar profile to a complex profile at Reynolds number around 500, suggesting a strong influence of flexible wall on flow transition.

The role of fluid viscoelasticity in the above-mentioned instability modes due to a flexible surface has received little attention. Earlier work was restricted to the role of viscoelasticity on the viscous mode in the limit of $\mathrm{Re} \to 0$. In most studies, the viscoelastic fluid is described either by the upper convected Maxwell (UCM) model or the Oldroyd-B model. For the creeping flow over a flexible surface, the fluid elasticity tends to either stabilize (suppression of instability) or delay the flow instability depending upon the values of viscoelasticity parameters [20–23]. Thus, introducing fluid elasticity is found to have a stabilizing influence on the Newtonian instability mode for $\mathrm{Re} \to 0$. The role of polymer addition in wall-mode instability at high Reynolds number for a flexible surface, as far as we know, has not been studied previously and is the subject of the present work.

In the present study, we investigate the wall-mode instability in flow of dilute polymer solution past a deformable solid in the limit of high Reynolds number. The linear stability analysis is carried out for the plane Couette flow of Oldroyd-B fluid past flexible surface. The rest of the paper is organized as follows. Section II provides the formulation for the stability analysis. The results for the viscoelastic wall modes are discussed in Sec. III A. In Sec. III C, the wall mode is continued to small Re in order to establish relationship between the viscous mode and the wall mode. Finally, the conclusions are summarized in Sec. IV.

II. PROBLEM FORMULATION

A. Governing equations

The base-flow configuration is linear velocity profile shown in Fig. 1. We nondimensionalize velocity with $\sqrt{G/\rho}$, distance with R, time with $R\sqrt{\rho/G}$, and pressure and stresses in fluid and wall with shear modulus G. The nondimensional fluid continuity and Cauchy momentum balance equations are

$$\nabla \cdot \mathbf{v} = 0, \tag{1}$$

$$D_t \mathbf{v} = -\nabla p^f + \nabla \cdot \boldsymbol{\tau}, \tag{2}$$

where $\mathbf{v}$ denotes the fluid velocity field and p^f is the fluid pressure. For the viscoelastic fluid modeled as an Oldroyd-B fluid, the total stress tensor $\boldsymbol{\tau}$ consists of viscous stress due to solvent $\boldsymbol{\tau}^s$ and the polymeric stress $\boldsymbol{\tau}^p$, $\boldsymbol{\tau} = \boldsymbol{\tau}^s + \boldsymbol{\tau}^p$. The viscous stresses arising due to the solvent viscosity η_s is given by the Newtons law of viscosity:

$$\boldsymbol{\tau}^s = \beta \frac{\Gamma}{\mathrm{Re}} [\nabla \mathbf{v} + (\nabla \mathbf{v})^T], \tag{3}$$

where $\Gamma = \sqrt{\rho V^2/G}$ is the dimensionless top-plate velocity. Physically, Γ is the ratio of inertial stresses in the fluid to the elastic stresses in the solid. The parameter $\beta = \eta_s/\eta$, known as the retardation parameter, is introduced to indicate the solvent contribution to the solution viscosity: $\eta = \eta_s + \eta_p$, where η_p is the measure of polymer contribution to the solution viscosity, indicated by $(1-\beta) = \eta_p/\eta$. The polymeric stress $\boldsymbol{\tau}^p$ is expressed with the help of dimensionless Oldroyd-B constitutive model:

$$\boldsymbol{\tau}^p + \mathrm{We}\, \mathcal{D}_t \boldsymbol{\tau}^p = (1-\beta) \frac{\Gamma}{\mathrm{Re}} [\nabla \mathbf{v} + (\nabla \mathbf{v})^T], \tag{4}$$

where T indicates transpose and Weissenberg number $\mathrm{We} = (\lambda/R)\sqrt{G/\rho}$ is the dimensionless relaxation time and is the

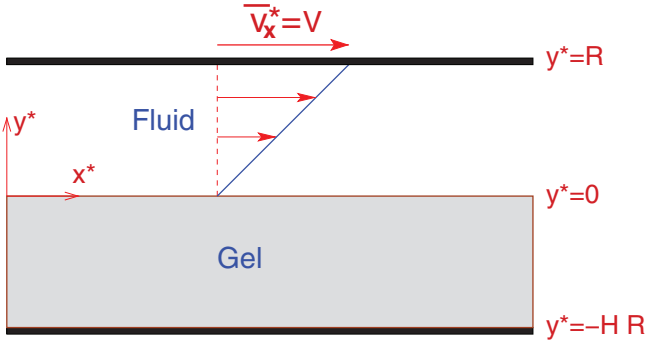

FIG. 1. (Color online) Schematic of plane Couette flow over a flexible surface showing a dimensional coordinate system.

measure of the elasticity of the viscoelastic fluid. Here λ is dimensional relaxation time of polymer solution. The material time derivative $\mathcal{D}_t\boldsymbol{\tau}^p$ is upper convected time derivative defined as

$$\mathcal{D}_t\boldsymbol{\tau}^p = \frac{\partial \boldsymbol{\tau}^p}{\partial t} + \mathbf{v}\cdot\nabla\boldsymbol{\tau}^p - \boldsymbol{\tau}^p\cdot(\nabla\mathbf{v}) - (\nabla\mathbf{v})^T\cdot\boldsymbol{\tau}^p. \quad (5)$$

Substituting the expressions of $\boldsymbol{\tau}^s$ and $\boldsymbol{\tau}^p$ in the momentum conservation equation (2), we get:

$$D_t\mathbf{v} = -\nabla p^f + \frac{\beta\Gamma}{\mathrm{Re}}\nabla^2\mathbf{v} + \nabla\cdot\boldsymbol{\tau}^p. \quad (6)$$

One recovers the governing equation for the Newtonian fluid in the limit either We $\to 0$ or $\beta = 1$. The upper convected Maxwell model (suitable for polymer melt) is obtained by setting $\beta = 0$.

The dynamics of the wall material is governed by the Hookean model for incompressible linearly elastic solid. The dynamics of the elastic solid medium is described by the displacement field $\mathbf{u}$, scaled by fluid thickness R, which represents the deviation of material points from their equilibrium position due to the fluid stresses. The dimensionless governing equations for solid continuum (referred to as gel) are

$$\nabla\cdot\mathbf{u} = 0, \quad (7)$$

$$D_t^2\mathbf{u} = -\nabla p_g + \nabla\cdot\boldsymbol{\sigma}. \quad (8)$$

Here p^g is the pressure in the solid material and $\boldsymbol{\sigma}$ the stress tensor for the wall. The stress tensor in wall medium is scaled by G, the shear modulus. The solid stress tensor in dimensionless form is given by the linear elastic constitutive model:

$$\boldsymbol{\sigma} = [\nabla\mathbf{u} + (\nabla\mathbf{u})^T]. \quad (9)$$

Here the viscous dissipation in the solid medium is ignored. While a nonlinear neo-Hookean model has been employed in previous studies on viscous instability [8,24,25], the nonlinear contribution is significant only when the base-state shear strain in the solid is greater than 1. In the present study, the strain in the elastic solid is of the order Γ^2/Re. For the wall-mode instability in the Newtonian fluid, the critical shear rate Γ_c scales as $\mathrm{Re}^{1/3}$ in the limit $\mathrm{Re} \gg 1$ [3], thus the magnitude of strain in the solid scales as $\mathrm{Re}^{-1/3}$, very small for $\mathrm{Re} \gg 1$. Hence, the linear elastic model can be used for wall-mode analysis. Indeed, the wall-mode analysis for the Newtonian fluid carried out by Chokshi and Kumaran [26] shows that the results for a neo-Hookean model are found to be same as that for the linear elastic model. As will be seen later, even for the polymeric fluids, the magnitude of shear strain in the solid medium remains smaller than 1, thus justifying the use of linear elastic model for the solid wall.

B. Base state

For the steady-state linear velocity profile, the fluid velocity, gel displacement, and stresses are given as:

$$\overline{\mathbf{v}} = (\Gamma y, 0, 0)$$

$$\overline{u}_x = \frac{\Gamma^2}{\mathrm{Re}}(y+H), \quad \overline{u}_y = 0, \quad \overline{u}_z = 0$$

$$\overline{\tau}_{xy} = \frac{\Gamma^2}{\mathrm{Re}}, \quad \overline{\tau}_{yy} = 0 \quad \overline{\tau}_{xx} = 2(1-\beta)\mathrm{We}\frac{\Gamma^3}{\mathrm{Re}}$$

$$\overline{\sigma}_{xy} = \frac{\Gamma^2}{\mathrm{Re}}, \quad \overline{\sigma}_{xx} = 0, \quad \overline{\sigma}_{yy} = 0,$$

$$\overline{p}_f = \overline{p}_g = \text{const.}$$

The base-flow solution satisfies the normal and tangential velocity and stress continuity conditions at the interface, which, for the base state, is flat at $y = 0$. Also, the no-slip condition for fluid velocity and zero displacement condition for solid are satisfied at top and bottom planes, respectively: $\mathbf{v} = (\Gamma,0,0)$ at $y = 1$ and $\mathbf{u} = (0,0,0)$ at $y = -H$.

C. Linear stability analysis

Two-dimensional perturbations of the following form are superimposed on the base-state flow:

$$\phi' = \tilde{\phi}(y)e^{ik(x-ct)}, \quad (10)$$

where k is streamwise wave number, c is complex wave speed, and ϕ represents any of the perturbation variable in fluid and solid, $\phi = [\mathbf{v}, p_f, \boldsymbol{\tau}, \mathbf{u}, p_g]$.

The linearized mass and momentum conservation equations for the fluid perturbation quantities $\tilde{\mathbf{v}}, \tilde{p}_f$ are

$$D\tilde{v}_y + ik\tilde{v}_x = 0, \quad (11)$$

$$ik(\Gamma y - c)\tilde{v}_x + \Gamma\tilde{v}_y = -ik\tilde{p}_f + \beta\frac{\Gamma}{\mathrm{Re}}(D^2-k^2)\tilde{v}_x + d_y\tilde{\tau}^p_{xy} + ik\tilde{\tau}^p_{xx}, \quad (12)$$

$$ik(\Gamma y - c)\tilde{v}_y = -D\tilde{p}_f + \beta\frac{\Gamma}{\mathrm{Re}}(D^2-k^2)\tilde{v}_y + D\tilde{\tau}^p_{yy} + ik\tilde{\tau}^p_{xy}. \quad (13)$$

Here D indicates d/dy. The disturbance in polymeric stress components $\tilde{\tau}^p_{ij}$ is governed by the linearized form of the Oldroyd-B equations:

$$\tilde{\tau}^p_{xx} + \mathrm{We}\left[ik(\Gamma y - c)\tilde{\tau}^p_{xx} - 4ik\mathrm{We}(1-\beta)\frac{\Gamma^3}{\mathrm{Re}}\tilde{v}_x - 2(1-\beta)\frac{\Gamma^2}{\mathrm{Re}}D\tilde{v}_x - 2\Gamma\tilde{\tau}^p_{xy}\right] = 2(1-\beta)\frac{\Gamma}{\mathrm{Re}}ik\tilde{v}_x, \quad (14)$$

$$\tilde{\tau}^p_{yy} + \mathrm{We}\left[ik(\Gamma y - c)\tilde{\tau}^p_{yy} - 2ik(1-\beta)\frac{\Gamma^2}{\mathrm{Re}}\tilde{v}_y\right] = 2(1-\beta)\frac{\Gamma}{\mathrm{Re}}D\tilde{v}_y, \quad (15)$$

$$\tilde{\tau}^p_{xy} + \mathrm{We}\left[ik(\Gamma y - c)\tilde{\tau}^p_{xy} - 2ik\mathrm{We}(1-\beta)\frac{\Gamma^3}{\mathrm{Re}}\tilde{v}_y - \Gamma\tilde{\tau}^p_{yy}\right] = (1-\beta)\frac{\Gamma}{\mathrm{Re}}(D\tilde{v}_x + ik\tilde{v}_y). \quad (16)$$

Substituting the expressions of the components of polymeric stress into the momentum conservation equations (12) and (13) and eliminating pressure, we get a single fourth-order

differential equation:

$$(1-\beta)[(S^2D^2 - 2ik\mathrm{We}\Gamma SD - 2k^2\mathrm{We}^2\Gamma^2 - k^2S^2) \times (D^2 - k^2 + 2ik\mathrm{We}\Gamma D - 2k^2\mathrm{We}^2\Gamma^2)\tilde{v}_y] + \beta S^3(D^2-k^2)^2\tilde{v}_y - ik\frac{\mathrm{Re}}{\Gamma}(\Gamma y - c)S^3(D^2-k^2)\tilde{v}_y = 0, \quad (17)$$

where $S = 1 + ik\mathrm{We}(\Gamma y - c)$.

The perturbation equations for the displacement field in the solid are

$$d_y\tilde{u}_y + ik\tilde{u}_x = 0, \quad (18)$$

$$-k^2c^2\tilde{u}_x = -ik\tilde{p}_g + (D^2-k^2)\tilde{u}_x, \quad (19)$$

$$-k^2c^2\tilde{u}_y = -D\tilde{p}_g + (D^2-k^2)\tilde{u}_y, \quad (20)$$

which can be combined to eliminate the pressure leading to a single equation:

$$(D^2-k^2)^2\tilde{u}_y + k^2c^2(D^2-k^2)\tilde{u}_y = 0. \quad (21)$$

The above governing equations are accompanied by the boundary conditions, vanishing perturbations of fluid velocity, and gel displacement field at the top and bottom rigid plates:

$$\tilde{v}_y(1) = \tilde{v}_x(1) = 0 \qquad \tilde{u}_y(-H) = \tilde{u}_x(-H) = 0. \quad (22)$$

At the perturbed interface with linearized unit normal $\mathbf{n} = (-\frac{\partial u'_y}{\partial x}, 1, 0)$, the normal and tangential velocity and stress continuity conditions hold. These conditions upon expanding in Taylor series around the flat interface ($y = 0$) give the following linearized interface conditions to be imposed at $y = 0$:

$$\tilde{v}_y = -ikc\tilde{u}_y, \quad (23)$$

$$\tilde{v}_x + \Gamma\tilde{u}_y = -ikc\tilde{u}_x, \quad (24)$$

$$\tilde{\tau}_{xy} - 2ik(1-\beta)\mathrm{We}\frac{\Gamma^3}{\mathrm{Re}}\tilde{u}_y = \tilde{\sigma}_{xy}, \quad (25)$$

$$-\tilde{p}_f + \tilde{\tau}_{yy} = -\tilde{p}_g + \tilde{\sigma}_{yy}. \quad (26)$$

In axial velocity continuity condition (24), the second term on the left-hand side is due to the jump in the steady-state shear rate across the fluid-solid interface. This term is known to be responsible for the low-Reynolds-number instability in flow past an elastic solid. The second term on the left-hand side of tangential stress continuity condition (25) is due to the jump in the first normal-stress difference N_1 across the fluid-solid interface. While normal stresses in the elastic solid are zero (for Hookean model), the Oldroyd-B viscoelastic fluid exhibits nonzero first normal-stress difference $N_1 = (\overline{\tau}_{xx} - \overline{\tau}_{yy}) = 2(1-\beta)\mathrm{We}\Gamma^3/\mathrm{Re}$ (refer to Sec. II B).

III. RESULTS AND DISCUSSION

A. Viscoelastic wall modes for Re ≫ 1

The shooting technique is applied to obtain the numerical solution of the fluid and solid governing equations [(17) and (21)] to be consistent with the top- and bottom-plate boundary conditions (22). The dispersion relation obtained by imposing the interface conditions [(23)–(26)] on the numerical solution results in a characteristic equation in terms of complex eigenvalue c, of the form:

$$\mathcal{F}(c, k, \mathrm{Re}, \Sigma, \beta, \mathrm{We}, H) = 0, \quad (27)$$

where $\Sigma = \rho G R^2/\eta^2$ is the flow independent dimensionless parameter characterizing the fluid-solid system. For a given fluid-solid system described by Σ, β, We, and H, setting the neutral stability condition of $c_i = 0$, we estimate the critical Reynolds number, Re_c, and disturbance wave speed, c_r:

$$(\mathrm{Re}_c, c_r) = \mathcal{G}(k, \Sigma, \beta, \mathrm{We}, H). \quad (28)$$

Next, the critical Reynolds number for the most unstable disturbance is obtained by finding the point of minimum Re_c in the Re_c-k plane. Finally, the neutral stability diagram is constructed in the Re_c-Σ plane.

First, we study the effect of fluid elasticity on Re_c corresponding to the most unstable Newtonian wall mode reported by Shankar and Kumaran [3] for $\Sigma = 5000$, $\beta = 0.5$, $k = 1$ and for different solid thickness H, as shown in Fig. 2. Upon continuation of the Newtonian wall mode for $H = 2$, the critical Reynolds number increases with We, indicating the stabilizing role of fluid elasticity for low values of the Weissenberg number. For highly elastic fluid with $\mathrm{We} \gg 1$, Re_c becomes independent of Weissenberg number and attains a plateau value. This stabilizing effect of fluid elasticity for $H = 2$ is in stark contrast to the destabilizing influence of an increasing Weissenberg number for $H = 3$, as shown in Fig. 2. Here the Re_c for the Newtonian wall mode first decreases upon increasing We, indicating the destabilizing influence of fluid elasticity. This viscoelastic wall mode with reduced value of Re_c exists up to a Weissenberg number ($\mathrm{We} \approx 30$). The numerical continuation of the lower branch for different thickness ratio H reveals a complex dependence on the parameters in the stability diagram. As seen in this figure, for $H = 2$, there exist two disconnected parts in the

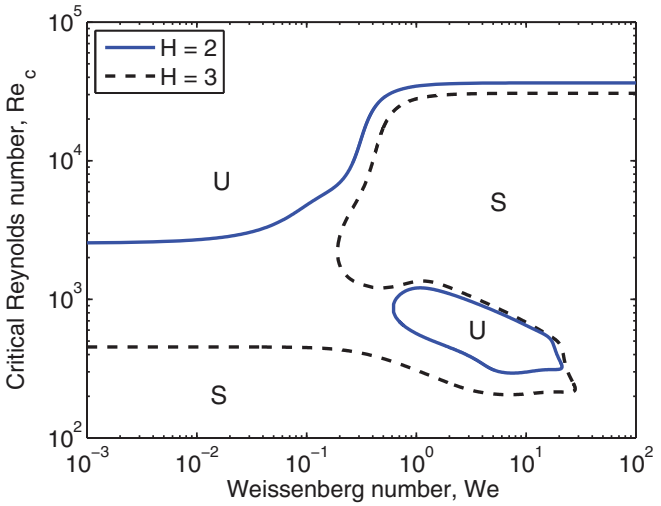

FIG. 2. (Color online) Effect of fluid elasticity on Newtonian wall mode: critical Reynolds number Re_c as a function of Weissenberg number We for $\Sigma = 5000$, $\beta = 0.5$, $k = 1$ and different values of solid thickness H. S denotes a stable region and U denotes an unstable region.

Re_c-We plane. While the upper part is a continuation of the Newtonian wall mode for viscoelastic fluid, the lower isolated domain of instability is constructed by continuation of the lower part for $H = 3$. The lower domain shrinks upon reducing the gel thickness. It is important to note here that the stability diagram in Fig. 2 is constructed for disturbance with wave number $k = 1$. As this disturbance may not be the most critical disturbance for transition, the quantitative findings will not be useful in later analysis. However, the important finding is that there exist two kinds of modes, one stabilizing (Re_c greater than Newtonian value) and the other destabilizing (Re_c less than Newtonian value), depending upon the thickness ratio H and Weissenberg number We.

It is more informative to estimate the value of critical Reynolds number Re_c corresponding to the most critical disturbance with wave number $k = k_c$. The critical point (k_c, Re_c) is obtained by locating the point of minimum Re when plotted against k. Figure 3 shows a typical plot. For Newtonian fluid with $\beta = 1$, the neutral stability curve has a clear point of minimum Re_c. Interestingly, for $\beta = 0.95$, indicating a dilute solution, the minimum Re_c is higher than its Newtonian value, highlighting the stabilizing effect of polymer addition with negligible change in solvent viscosity. For $\beta = 0.5$, the two dissociated parts of the neutral stability curve correspond to the upper instability curve and lower isolated domain of instability shown earlier in Fig. 2. As seen, the lower part encloses with itself and does not exist beyond a range of wave numbers. Clearly, the critical point in the Re_c-k plane occurs in the lower domain, where it exists, and the critical perturbation has wave number $k_c \sim O(1)$. Thus, for $\beta = 0.5$, the critical Reynolds number for instability Re_c is lower than its value for the Newtonian fluid, indicating the destabilizing role of polymer addition for a concentrated solution. On the other hand, for dilute solution, represented by parameter $\beta = 0.95$, the lower isolated domain does not exist for $\Sigma = 5000$, hence,

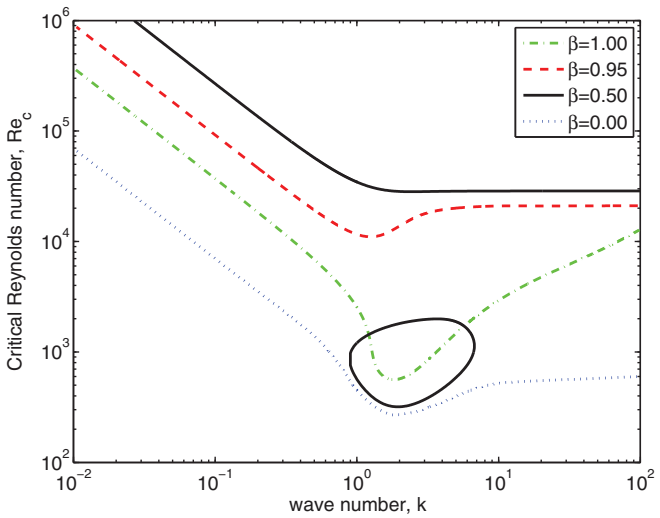

FIG. 3. (Color online) Variation of critical Reynolds number Re_c with disturbance wave number for $\Sigma = 5000$, $H = 2.0$, We $= 1.0$, and different values of β. The point of minimum Γ_t on this curve represents the critical point (k_c, Γ_c). The curve for $\beta = 1$ represents the Newtonian wall mode.

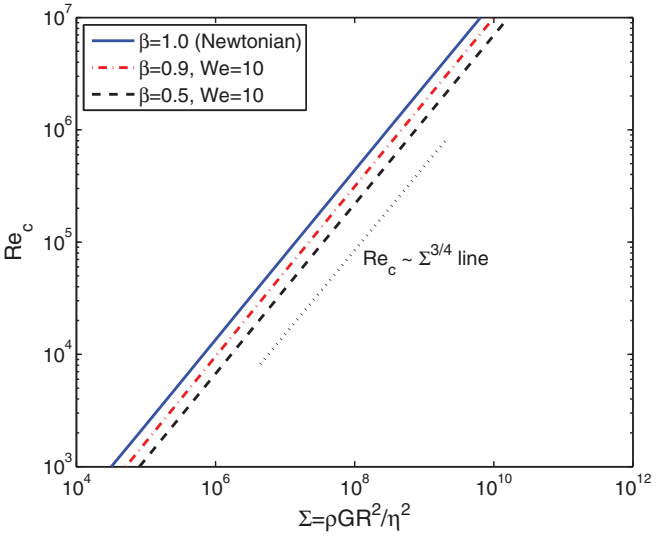

FIG. 4. (Color online) Neutral stability curve showing the critical Reynolds number as function of dimensionless parameter Σ for $H = 5$ and for varying values of β. Polymer addition (decreasing β below unity) tends to reduce Re_c for a given value of Σ. Viscoelastic wall-mode instability follows the scaling law $\mathrm{Re} \sim \Sigma^{3/4}$.

the polymer addition tends to increase Re_c, a stabilizing effect. Thus, the polymer addition plays a dual role on the critical Reynolds number for instability. While the dilute solution ($\beta = 0.95$) tends to increase Re_c, the concentrated solution reduces the critical Reynolds number from its Newtonian value.

The critical Reynolds number Re_c obtained for $\Sigma = 5000$ is now continued to higher values of Σ and the neutral stability diagram is constructed in the Re_c-Σ plane such that all along the stability curve the Reynolds number is Re_c and the wave number is k_c, the point of the global minimum in the Re-k plane. Figure 4 shows one such diagram for $H = 5$ and different values of β. In this figure, we use $H = 5$ in place of $H = 2$ used in previous plots, only for clarity, as for thicker solids the role of polymer addition becomes more pronounced. The curve for $\beta = 1$ is for the Newtonian wall mode and is shown for comparison. It is evident that for $\beta \geqslant 0.9$, the stability curve for the polymeric fluid lies below the curve for the Newtonian fluid. Thus, for a given fluid-solid system characterized by Σ, the critical Reynolds number for instability, Re_c, decreases upon reducing β from $\beta = 1$ to $\beta = 0.9$ and 0.5. Thus, increasing the concentration of polymer has a destabilizing influence on the wall mode of instability. Moreover, the critical Reynolds number is found to follow the Newtonian scaling $\mathrm{Re} \sim \Sigma^{3/4}$. This shows that the viscoelastic wall mode is qualitatively similar to the Newtonian wall mode. Figure 5 shows stability curves for different values of Oldroyd-B model parameters β and We for $H = 5$. It is seen that for varied values of β and elasticity, the neutral stability curve for the viscoelastic fluid follows the universal scaling of $\mathrm{Re} \sim \Sigma^{3/4}$. Also, the destabilizing role of viscoelasticity is evident as stability curves for the viscoelastic wall mode stay below that for the Newtonian wall mode. Figure 6 shows the stability diagrams for different values of solid thickness.

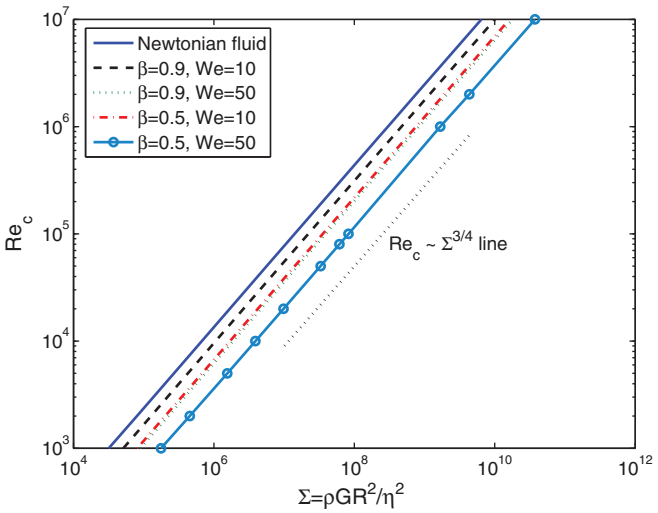

FIG. 5. (Color online) Stability diagram in the Re_c-Σ plane for $H = 5$ and varying values of β and We. The destabilizing role of fluid elasticity is evident. For different values of viscoelasticity parameters Re_c scales as $\Sigma^{3/4}$.

As discussed earlier with the help of Figs. 2 and 3, the viscoelasticity exhibits two kinds of unstable modes: one attributed to the lower isolated domain (which has a destabilizing role of polymer) and the other which shows the stabilizing effect of elasticity. The latter mode exists in most cases. In cases where the lower domain exists, the *critical mode* lies below the Newtonian wall mode, suggesting the destabilizing influence of viscoelasticity as shown in the above-discussed stability diagrams. To demonstrate the opposite role of viscoelasticity, Fig. 7 shows the stability diagram for $H = 0.5$ and $\beta = 0.95$ for which case the lower isolated domain disappears at least for low Reynolds number (around 1000). In this case, the upper structure is the only mode and hence critical. Upon continuing this mode to

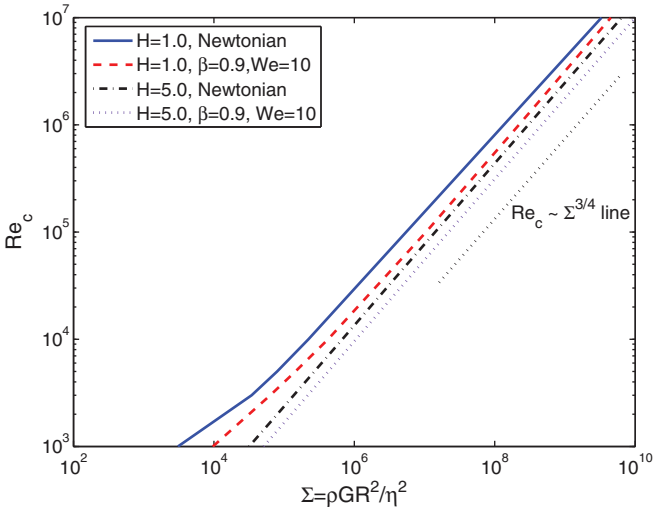

FIG. 6. (Color online) Effect of wall thickness H on critical Reynolds number for $\beta = 0.9$ and $\mathrm{We} = 10$. Thicker the solid the lower the critical Reynolds number.

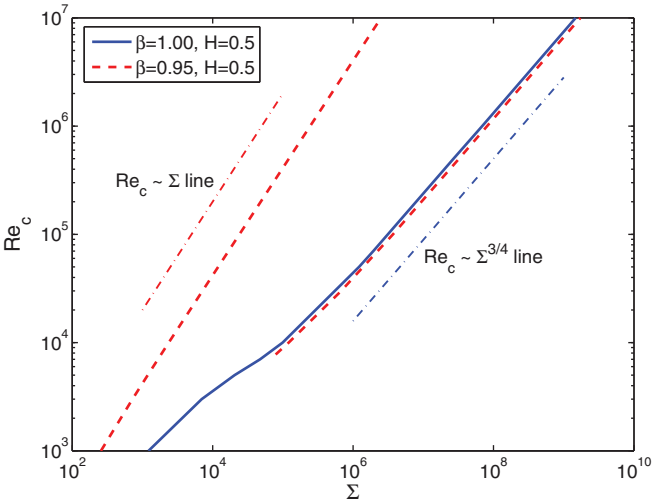

FIG. 7. (Color online) Neutral stability curve in the Re_c-Σ plane for $H = 0.5$. The broken lines are for $\beta = 0.95$, representing a very dilute solution. The dual role of polymer addition is visible. The upper branch which follows $\mathrm{Re}_c \sim \Sigma$ exists for all Reynolds number. At $\mathrm{Re} \approx 7760$, the lower branch appears and it is the most critical mode higher Reynolds number. For $\mathrm{Re} \lesssim 7760$, the role of the polymer is strongly stabilizing.

higher Reynolds number, the stability curve remains above the Newtonian curve. Interestingly, this mode of instability follows the scaling $\mathrm{Re}_c \sim \Sigma$, a departure from the Newtonian wall mode behavior. Upon increasing Re, the lower isolated domain first appears at $\mathrm{Re} \approx 7760$. Hence, the stability curve, constructed by the loci of the global minimum on the lower isolated domain at a Reynolds number higher than $\mathrm{Re} \approx 7760$, determines the stability of the system. This curve, as shown in Fig. 7, lies marginally below the Newtonian curve and follows the Newtonian scaling law of $\mathrm{Re} \sim \Sigma^{3/4}$. Thus, of the two curves shown for $\beta = 0.95$, the bottom one, indicating the destabilizing influence of polymer addition, is the real critical stability curve for any $\mathrm{Re} \gtrsim 7760$. For $\beta \lesssim 0.95$, the lower isolated domain is present even at $\mathrm{Re} = 1000$. Thus, the neutral stability curves for $\beta < 0.95$ would stay below the Newtonian curve (not shown). It is observed that the lower isolated domain grows bigger upon increasing the Reynolds number, and it shrinks and disappears upon reducing the Reynolds number.

To summarize, the continuation of the most unstable Newtonian wall mode for shear flow past a compliant surface of a viscoelastic fluid reveals that, for thick solids ($H \gtrsim 1$), the fluid elasticity has a destabilizing effect on the Newtonian wall mode for full range of parameter β (all concentration levels of polymer addition) and the viscoelastic wall mode follows the scaling law of $\mathrm{Re}_c \sim \Sigma^{\alpha}$ for $\mathrm{Re} \gg 1$ with exponent $\alpha \approx 3/4$. On the other hand, for thin solids ($H \lesssim 1$), the fluid elasticity has stabilizing influence on the Newtonian wall mode for very dilute polymer solution ($0.8 \lesssim \beta < 1$) and the influence is destabilizing for $\beta \lesssim 0.8$. Here the stabilizing influence is accompanied by the power-law exponent $\alpha \approx 1$, and the destabilizing effect by $\alpha \approx 3/4$. This summary holds for most practical dilute polymeric solutions with $\mathrm{We} \lesssim 100$. Figure 8 shows the schematic illustration of this summary in the β-H domain, plotted for $\mathrm{Re} \approx 1100$. As mentioned

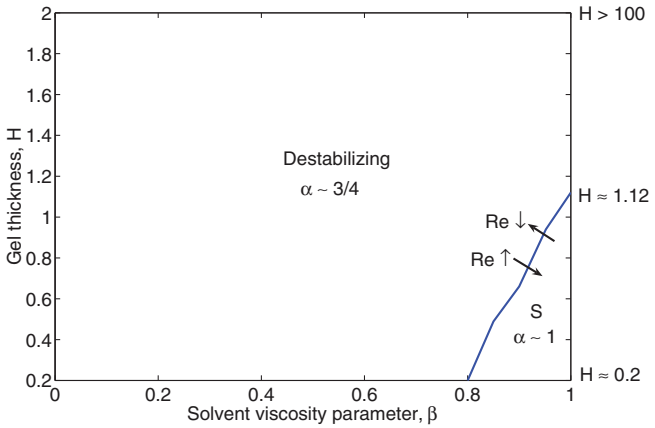

FIG. 8. (Color online) Schematic diagram showing qualitatively the region of stabilizing and destabilizing effects of polymer addition on the least stable Newtonian wall mode in β-H space valid for Re $\approx$ 1100 and any Weissenberg number under 100. Here S denotes stabilizing influence and α is the exponent in the power-law scaling Re $\sim \Sigma^{\alpha}$.

before, the lower isolated domain grows upon increasing the Reynolds number, hence the region in the β-H space with a destabilizing influence also grows with the Reynolds number. The stabilizing role of polymer addition, on the other hand, can be seen in a region of dilute polymer solution, which grows upon decreasing the Reynolds number. It should be noted that the words "stabilizing" and "destabilizing" mean respective increase or decrease of the critical Reynolds number by polymer addition in comparison to the Newtonian value of Re_c.

B. Viscoelastic wall-mode scaling

In this section, we comment on the scalings observed for the viscoelastic wall modes. The two characteristic scalings for the most unstable wall mode are Re $\sim \Sigma^{3/4}$ and Re $\sim \Sigma$ in the limit Re $\gg 1$. The former is the characteristic scaling for the wall modes for Newtonian fluids [3]. Here there exists a thin layer of thickness $\delta \sim \mathrm{Re}^{-1/3}$ close to the fluid-solid interface where the disturbance vorticity is confined. In the leading order, the viscous, polymeric and inertial stresses are of comparable magnitude within this wall layer, giving viscoelastic wall modes as solution for the disturbance growth rate. The unstable wall modes for the polymeric fluids are qualitatively similar to the Newtonian wall modes confining the role of polymer to quantitative modification of the critical Reynolds number, which is found to be the reduction in Re_c (destabilizing role).

The other scaling of Re $\sim \Sigma$ for Re $\gg 1$ suggests a thin layer of thickness $\delta \sim \mathrm{Re}^{-1/2}$ located on the fluid side of the fluid-solid interface. A balance of various terms in the disturbance momentum balance equation shows that at the leading order the viscous and polymeric stresses within this layer are comparable and are $O(\mathrm{Re}^{1/2})$ larger than the inertial forces. We refer to this layer as the *elastic layer*. Therefore, while inertial, viscous, and polymeric forces are comparable within a wall layer of thickness $l \sim O(\mathrm{Re}^{-1/3})$, there exists an elastic sublayer of thickness $O(\mathrm{Re}^{-1/2})$ within this wall layer where the viscous and polymeric forces are comparable and are stronger than the inertial forces. Since the polymeric stresses are time dependent, the leading-order growth rate can be found by solving the inertialess equation at the leading order. These modes qualitatively differ from the Newtonian wall modes and exist only for the viscoelastic fluids.

C. Relationship between the wall mode and the viscous mode

The viscous mode analysis for the Oldroyd-B fluid past a Hookean solid in the limit Re $\ll 1$ had been carried out by Chokshi and Kumaran [22]. In this section, we endeavor to relate the wall modes analyzed in Sec. III A for Re $\gg 1$ to the viscous mode instability for Re $\ll 1$. It is obvious that one cannot use the same nondimenionalization scheme in both regimes. For viscous flow, the appropriate time scale is η/G obtained by balancing viscous stresses in fluid with the elastic stresses in the solid. This gives the dimensionless shear rate, which is the critical parameter for instability, to be defined as $\overline{\Gamma} = V\eta/(GR)$, and flow Weissenberg number $\overline{\mathrm{We}} = \lambda G/\eta$. These quantities are related to Γ and We using the equalities $\overline{\Gamma} = \Gamma^2/\mathrm{Re}$ and $\overline{\mathrm{We}} = \mathrm{WeRe}/\Gamma$.

Figure 9(a) shows the transition shear rate $\overline{\Gamma}_t$ (may also be termed as the critical shear rate) for varying fluid elasticity at Re $= 1000$ (the wall mode), which is similar to the plot in the Re-We plane shown in Fig. 2. A similar curve for Re $\to 0$ (the viscous mode) is shown in Fig. 9(b) for the same set of parameters [22]. One can see that the upper part of the plot for wall mode has nearly the same value of $\overline{\Gamma}_t$ as that shown in the plot for viscous mode. Thus, the upper branch, which signifies the stabilizing effect of viscoelasticity, at high Reynolds number is simply the continuation of the viscous mode. Interestingly, the numerical value of $\overline{\Gamma}_t$ is not much affected as Reynolds number is decreased from 1000 to close to zero. Now, the lower isolated domain for the wall mode, which shows the destabilizing effect of fluid elasticity, appears to shrink upon decreasing Reynolds number, such that it is absent in the limit Re $\to 0$. Thus, for any given set of parameters, the lower isolated domain always shrinks and ceases to exist at a certain low value of Reynolds number, where as it always exists in the limit Re $\gg 1$. A typical case is for $H = 0.5$ shown earlier in Fig. 7, where the lower isolated domain disappears below Re ≈ 7760. It is observed that the thicker the solid, the lesser is the value of Reynolds number where the lower branch disappears. Note that the lower branch, whenever it exists, represents the most unstable mode with lowest transition shear rate and it exhibits the destabilizing effect of fluid elasticity. For this mode, $\mathrm{Re}_c \sim \Sigma^{3/4}$ in the limit Re $\gg 1$ (see Fig. 8), and it does not continue for Re $\ll 1$. Thus, the most unstable wall mode for the viscoelastic fluid does not continue to the viscous mode. This finding is contrary to the Newtonian fluid for which case the most unstable wall mode is numerical continuation of the unstable viscous mode [3].

To further confirm the above arguments, the numerical continuation of wall mode to small Reynolds number is shown in Fig. 10(b) for $\overline{\mathrm{We}} = 100$. As expected, the upper branch continues to small Re with $\overline{\Gamma}_t$ independent of Re, whereas the two branches corresponding to the lower isolated domain merge with each other and hence do not continue to small Re. Thus, the lower part in the diagram for wall mode, which,

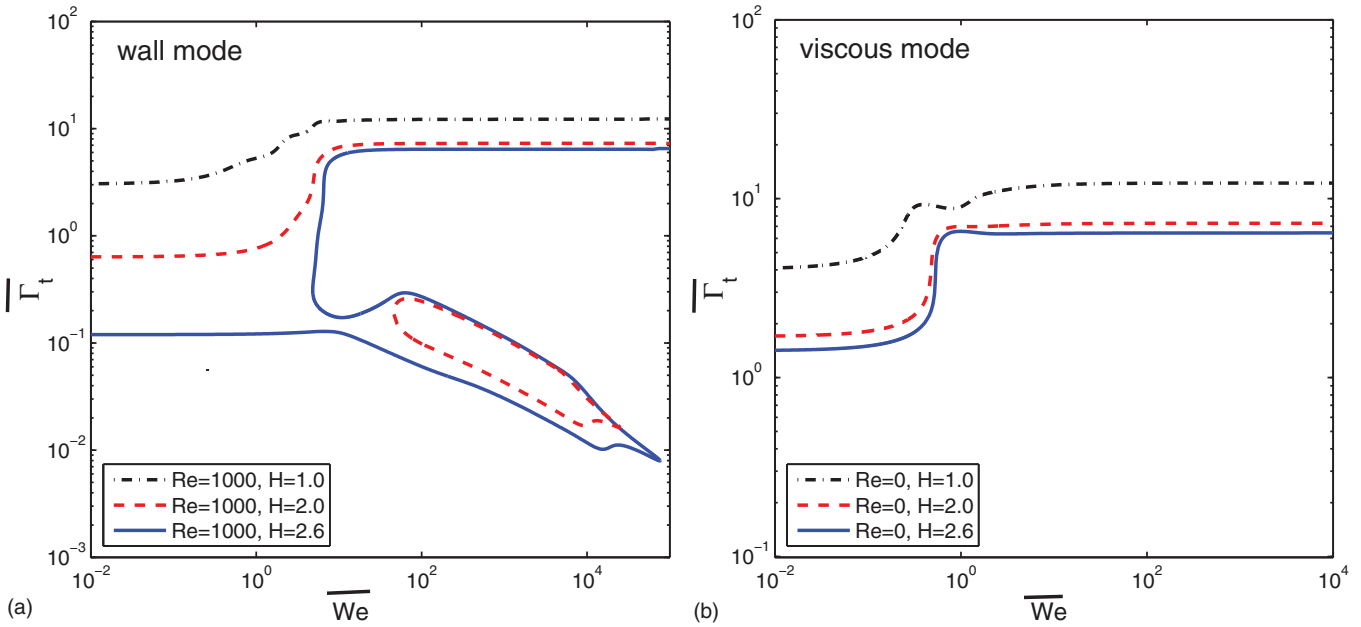

FIG. 9. (Color online) Neutral stability curve in the $\overline{\Gamma}_t$-$\overline{\mathrm{We}}$ plane for $k = 1$, $\beta = 0.5$ and different values of H. (a) For wall mode at $\mathrm{Re} = 1000$. (b) For viscous mode at $\mathrm{Re} \to 0$. The upper branch for the wall mode has the same value as the viscous mode for $\overline{\mathrm{We}} > 1$.

at very high Re, accounts for, first, the destabilizing effect of polymer addition and, second, the exponent $\alpha \sim 3/4$ in the power-law relation $\mathrm{Re}_c \sim \Sigma^{\alpha}$ disappears upon reducing the Reynolds number. This is consistent with the observation made in Sec. III A that the lower isolated domain shrinks and disappears upon reducing the Reynolds number. Hence, at small Re, the polymer addition has only the stabilizing effect on the Newtonian mode, whereas for $\mathrm{Re} \gg 1$, the lower isolated domain appears, indicating destabilizing effect of polymer on Newtonian wall mode.

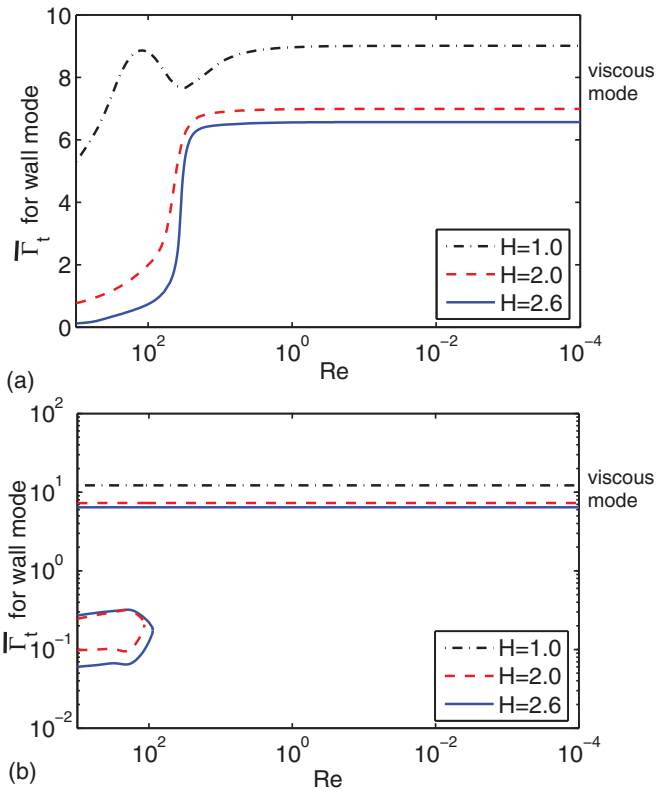

FIG. 10. (Color online) Continuation of wall mode in Fig. 9 to $\mathrm{Re} \ll 1$. (a) For $\overline{\mathrm{We}} = 1$; (b) for $\overline{\mathrm{We}} = 100$. Two lower branches merge and disappear while upper branch continues to viscous mode.

D. Inviscid instability

Before concluding our present study on wall-mode instability, we present a brief note on an observation made during the present analysis. The observation is about the inviscid instability for the flow of a Newtonian fluid past a flexible surface. In the inviscid instability, there exists a wall layer of thickness $O(\mathrm{Re}^{-1/2})$ smaller than the channel width in the regime $\mathrm{Re} \gg 1$. In this layer, the inertial stresses in the fluid are balanced by the elastic stresses in the wall, such that $(\rho V^2/G) \sim 1$. The viscous stresses in this layer are $O(\mathrm{Re}^{-1/2})$ smaller than the inertial stresses. This class of modes are referred to as *inviscid modes*. It is important to note that the wall modes are qualitatively distinct from the inviscid modes. Based on the asymptotic analysis [1,27], it is shown that the inviscid modes are always stable for the plane Couette flow and also for the parabolic profile in a flexible tube. If found unstable, the critical Reynolds number for the inviscid modes scales as $\mathrm{Re}_c \sim \Sigma^{1/2}$ in the limit $\mathrm{Re} \gg 1$ which is lower than that for the wall-mode instability, $\mathrm{Re} \sim \Sigma^{3/4}$. Therefore, the inviscid modes are more unstable than the wall modes.

While the asymptotic analysis suggests stable inviscid modes, the numerical calculations performed in the present study found an instability which follows the typical scalings of inviscid modes. Figure 11 plots the critical Reynolds number against Σ for the Newtonian fluid. The most unstable wall mode follows the scaling of $\mathrm{Re}_c \sim \Sigma^{3/4}$. However, there exists another stability curve, lying below the wall-mode curve, which follows the scaling $\mathrm{Re}_c \sim \Sigma^{1/2}$, indicating an "inviscid"

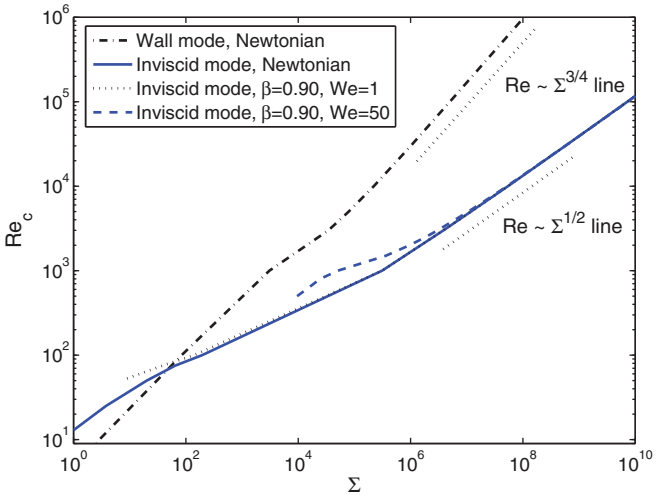

FIG. 11. (Color online) Stability diagram for the unstable inviscid mode for $H = 5$. The inviscid instability mode is seen to be more unstable than the most unstable wall mode and follows the scaling law $\mathrm{Re} \sim \Sigma^{1/2}$. The inviscid instability is unaffected by fluid elasticity.

instability mode. Since the mechanism of inviscid instability is due to Reynolds's stresses and pressure forces acting on the fluid-solid interface, the polymeric stresses are expected to play no role. This is shown in Fig. 11, where the fluid elasticity has a negligible effect on the inviscid instability.

To further examine the occurrence of inviscid instability *before* the wall-mode instability, we plot in Fig. 12(a) the disturbance growth rate (which is the imaginary part of complex wave speed, c) against the dimensionless shear rate Γ. As shown, the growth rate first becomes positive for $\Gamma \approx 2$, which is the inviscid instability. However, upon further increasing the shear rate, the growth rate turns negative and for $\Gamma \approx 100$, the wall-mode instability sets in, making the growth rate again positive. The wall-mode instability persists for any large value of Γ. Importantly, the value of growth rate for inviscid instability is very small in comparison to the wall-mode instability. For high Reynolds number, the growth rate, however positive, becomes very small, indicating marginal (or weak) instability.

In order to confirm the numerical existence of the inviscid instability, we have carried out an asymptotic analysis in the limit $\mathrm{Re} \gg 1$ using $\delta = \mathrm{Re}^{-1/2}$ as the small parameter. The methodology is similar to that explained in Kumaran [1]. The details are omitted for brevity. At the leading order, the complex wave speed comes out to be a real quantity, with a zero imaginary part, indicating that the flow is neutrally stable. At the first order, $O(\delta)$, the complex wave speed has a negative imaginary part for all values of imposed shear rate Γ, as shown in Table I. Thus, the flow is stable to the inviscid mode. The second-order correction to the growth rate, however, becomes positive at a certain value of Γ. The complex wave speed is given by an asymptotic expansion: $c = c^{(0)} + \delta c^{(1)} + \delta^2 c^{(2)}$, where $\delta = \mathrm{Re}^{-1/2}$. Figure 12(b) shows a comparison of the numerical results for growth rate c_i with the asymptotic results for $\mathrm{Re} = 10^6$. While the trend is in qualitative agreement, unlike the numerical results, the growth rate obtained from the asymptotic analysis never becomes positive. The difference,

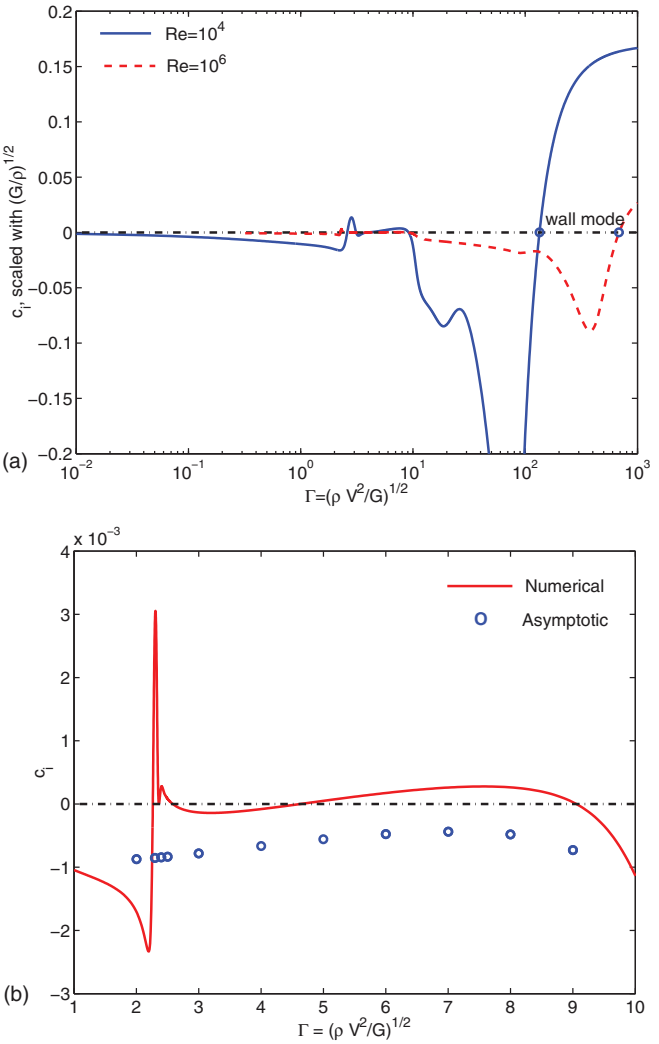

FIG. 12. (Color online) Variation of growth rate with shear rate Γ for Newtonian fluid flow at high Reynolds number for $H = 1$ and $k = 1$. (a) Numerical results for $\mathrm{Re} = 10^4$ and $\mathrm{Re} = 10^6$. Both inviscid-mode and wall-mode instability are shown. (b) Asymptotic results are compared with the numerical results for growth rate for $\mathrm{Re} = 10^6$. While the numerical growth rate is positive for a range of Γ, the asymptotically calculated growth rate remains negative, indicating stable inviscid mode.

however, is very small, of the order of 10^{-3}. It should be emphasized that the instability is not because of any numerical error, as numerical results are independent of grid size as adaptive step size control has been employed. Finally, since the magnitude of the growth rate for inviscid instability is very small, and the range of shear rate for which the growth rate remains positive is very narrow, this instability may be termed as marginal or weak, and its realization in physical setup is questionable.

IV. CONCLUSIONS

The stability of plane Couette flow of an Oldroyd-B viscoelastic fluid over a flexible surface has been analyzed with the focus on dilute polymer solution at high Reynolds number. In the limit $\mathrm{Re} \gg 1$, there exists a wall layer of

TABLE I. Inviscid-mode asymptotic analysis in the limit $\mathrm{Re} \gg 1$; $c = c^{(0)} + \delta c^{(1)} + \delta^2 c^{(2)}$, where $\delta = \mathrm{Re}^{-1/2}$ and $\Gamma \sim 0(1)$. Numerical value of c is provided for $\mathrm{Re} = 10^6$.

Γ	$c^{(0)}$	$c^{(1)}$	$c^{(2)}$	Numerical c
2.0	$(2.15094 + 0i)$	$(-0.87195 - 0.87195i)$	$(0 - 0.16407i)$	$(2.14919 - 0.0017034i)$
2.3	$(2.21781 + 0i)$	$(-0.85225 - 0.85225i)$	$(0 + 0.03340i)$	$(2.21404 + 0.0029634i)$
2.4	$(2.24045 + 0i)$	$(-0.84402 - 0.84402i)$	$(0 + 0.11113i)$	$(2.23853 + 0.0002700i)$
2.5	$(2.26325 + 0i)$	$(-0.83513 - 0.83513i)$	$(0 + 0.19446i)$	$(2.26156 + 0.0000841i)$
3.0	$(2.37978 + 0i)$	$(-0.78348 - 0.78348i)$	$(0 + 0.68734i)$	$(2.37836 - 0.0001336i)$
4.0	$(2.62458 + 0i)$	$(-0.66636 - 0.66636i)$	$(0 + 1.95874i)$	$(2.62333 - 0.0000807i)$
5.0	$(2.88336 + 0i)$	$(-0.55888 - 0.55888i)$	$(0 + 3.42446i)$	$(2.88220 + 0.0000499i)$
6.0	$(3.15380 + 0i)$	$(-0.47968 - 0.47968i)$	$(0 + 4.90115i)$	$(3.15268 + 0.0001739i)$
7.0	$(3.43313 + 0i)$	$(-0.44428 - 0.44428i)$	$(0 + 6.20917i)$	$(3.43199 + 0.0002602i)$
8.0	$(3.71742 + 0i)$	$(-0.48642 - 0.48642i)$	$(0 + 6.86338i)$	$(3.71620 + 0.0002633i)$
9.0	$(3.99887 + 0i)$	$(-0.73302 - 0.73302i)$	$(0 + 4.11454i)$	$(3.99739 + 0.0000282i)$

thickness $O(\mathrm{Re}^{-1/3})$ smaller than the channel width in which the inertial and viscous stresses in fluid are comparable to the elastic stresses in the solid. This class of modes, known as wall modes, are unstable for Newtonian fluid. The role of fluid viscoelasticity, in terms of two Oldroyd-B parameters, the Weissenberg number We and the retardation parameter β, indicating the polymer concentration, are studied. For very high Reynolds number flow, the critical Reynolds number for the transition is lower for the viscoelastic fluid than its value for the Newtonian fluid. Thus, the fluid elasticity shows a destabilizing influence on the Newtonian wall mode. Moreover, the critical Reynolds number scales with $\Sigma = \rho G R^2/\eta^2$, the parameter characterizing the fluid-solid system, as $\mathrm{Re} \sim \Sigma^{3/4}$ for $\mathrm{Re} \gg 1$, the same as the Newtonian wall mode. This scaling holds for all values of β and We. However, for a moderate Reynolds number in the range of 10^3–10^4, the role of fluid elasticity can be either destabilizing or stabilizing in comparison to the the Newtonian fluid depending upon the dimensionless solid thickness H and the polymer concentration parameter β. For very dilute polymer solutions with $\beta = \eta_s/\eta$ just under unity ($0.9 \lesssim \beta < 1$) and for thin solids with $H \lesssim 1.1$, the above-mentioned branch with scaling $\mathrm{Re}_c \sim \Sigma^{3/4}$ (destabilizing role of polymer) disappears and the most unstable branch follows the scaling $\mathrm{Re}_c \sim \Sigma$, a departure from the Newtonian wall-mode behavior. This implies that the critical Reynolds number in this regime is higher for the viscoelastic fluid than its value for the Newtonian fluid. Thus, a very small addition of polymer molecules tends to delay the transition, indicating a stabilizing role of fluid elasticity.

Except for a narrow region of parameters in β-H space, increasing fluid elasticity renders the wall modes more unstable. This destabilizing role of polymer at high Reynolds number wall modes is contrary to the stabilizing effect of elasticity in the viscous mode in the absence of inertia. It has been shown that the most unstable viscoelastic wall mode at high Reynolds number ceases to exist when the Reynolds number is decreased, thus it does not continue to the viscous mode. This behavior differs from the Newtonian case, where the most unstable wall mode is numerical continuation of the viscous mode.

The instability predicted in the present study can be realized experimentally for a plane shear flow of polymeric fluid over a deformable elastic solid. In similar experiments conducted earlier [9,11,18,19], the shear modulus of flexible surface G is around 10^3–10^4 N/m^2. As the emphasis of the present study is on the dilute polymer solution, the material properties can be that of water or organic liquid, i.e., $\rho \approx 10^3$ kg/m^3 and $\eta \approx 10^{-3}$ Pa s. A polymer concentration of less than 2% vol does not significantly alter the viscosity, suggesting $\beta \sim$ 0.7–0.9. For a channel width of 1 mm and solid thicknesses of 1–5 mm, the parameter $\Sigma \approx 10^6$–10^7. For $\Sigma \approx 10^6$, the critical Reynolds number for Newtonian fluid is around 10^4. By adding a polymer chain in concentrations of 2% vol (corresponding to $\beta = 0.95$) or higher, the instability can be realized at Re_c of around 1000 (an order of magnitude lower than its Newtonian value). For this, a Weissenberg number of around 50 corresponds to chains with relaxation time in the range 0.01–0.05 s. Higher relaxation time will show a further drop in critical Reynolds number below 1000. This value of Re_c is attainable in experiments, thus the dual role of the polymer additive may be observed in experimental conditions.

Interestingly, we also report the existence of series of unstable modes for which the critical Reynolds number for transition is much lower compared to that for the wall modes, of the order of $\mathrm{Re}_c \sim \Sigma^{1/2}$ for $\Sigma \gg 1$. The eigenfunction for this class of modes follows the scaling of inviscid modes, which were reported to be stable for the plane Couette flow based on asymptotic analysis [1,27]. However, the small magnitude of the disturbance growth rate for these modes makes them only marginally unstable and hence unlikely to be observed in a channel of finite length with finite residence time.

[1] V. Kumaran, J. Fluid. Mech **302**, 117 (1995).
[2] L. Srivatsan and V. Kumaran, J. Phys. II France **7**, 947 (1997).
[3] V. Shankar and V. Kumaran, Phys. Fluids **14**, 2324 (2002).
[4] P. Krindel and A. Silberberg, J. Colloid Interface Sci. **71**, 39 (1979).

[5] V. Kumaran, Current Science **79**, 766 (2000).
[6] V. Kumaran, G. H. Fredrickson, and P. Pincus, J. Phys. II France **4**, 893 (1994).
[7] V. Kumaran, J. Fluid. Mech. **294**, 259 (1995).
[8] V. Gkanis and S. Kumar, J. Fluid Mech. **524**, 357 (2005).
[9] R. Muralikrishnan and V. Kumaran, Phys. Fluids **14**, 775 (2002).
[10] V. Kumaran and R. Muralikrishnan, Phys. Rev. Lett. **84**, 3310 (2000).
[11] M. D. Eggert and S. Kumar, J. Colloid Interface Sci. **278**, 234 (2004).
[12] G. M. Corcos and J. R. Sellars, J. Fluid Mech. **5**, 97 (1959).
[13] A. E. Gill, J. Fluid Mech. **21**, 145 (1965).
[14] A. E. Gill, J. Fluid Mech. **21**, 503 (1965).
[15] V. Shankar and V. Kumaran, Euro. Phys. J. B **19**, 607 (2001).
[16] V. Kumaran, J. Fluid. Mech **357**, 123 (1998).
[17] V. Kumaran, J. Fluid. Mech **362**, 1 (1998).
[18] M. K. S. Verma and V. Kumaran, J. Fluid Mech. **705**, 322 (2012).
[19] M. K. S. Verma and V. Kumaran, J. Fluid Mech. **727**, 407 (2013).
[20] V. Shankar and S. Kumar, J. Non-Newtonian Fluid Mech. **116**, 371 (2004).
[21] S. Kumar and V. Shankar, J. Non-Newtonian Fluid Mech. **125**, 121 (2005).
[22] P. Chokshi and V. Kumaran, Phys. Fluids **19**, 034102 (2007).
[23] P. Chokshi and V. Kumaran, Phys. Fluids **19**, 104103 (2007).
[24] V. Gkanis and S. Kumar, Phys. Fluids **15**, 2864 (2003).
[25] P. Chokshi and V. Kumaran, Phys. Rev. E. **77**, 056303 (2008).
[26] P. Chokshi and V. Kumaran, Phys. Fluids **20**, 094109 (2008).
[27] V. Shankar and V. Kumaran, J. Fluid Mech. **395**, 211 (1999).